Electron Spin−Lattice Relaxation Measurement of the 3Fe-4S (S-3) Cluster in Succinate:Ubiquinone Reductase from *Paracoccus Denitrificans*. A Detailed Analysis Based on a Dipole−Dipole Interaction Model

Shao-Ching Hung,[†] Christopher V. Grant,[‡] Jeffrey M. Peloquin,[‡] A. Reginald Waldeck,[†,§] R. David Britt,[‡] and Sunney I. Chan*[,†]

Arthur Amos Noyes Laboratory of Chemical Physics 127-72, California Institute of Technology, Pasadena, California 91125, and the Department of Chemistry, University of California, Davis, California 95616

Received: October 18, 1999; In Final Form: January 20, 2000

The electron spin−lattice relaxation for the 3Fe-4S (S-3) center in succinate:ubiquinone reductase has been examined using both inversion recovery and "picket-fence" pulse sequences at a temperature range of 4−8 K. The latter pulse sequence is used to eliminate the interference of spectral diffusion in frozen solids. An abnormally fast relaxation was observed for the S-3 center. We attribute this rapid relaxation to a magnetic dipolar interaction between the S-3 center and a nearby paramagnetic *b*-heme (cytochrome *b*). A model has been developed to treat the interaction between two paramagnetic redox centers in a rigid lattice at a fixed distance apart but with random orientations in a magnetic field. Both the contribution to the spin−lattice relaxation rate from the dipolar interaction ($k_{1\theta}$), which is anisotropic, and the intrinsic electron spin relaxation, which is scalar ($k_{1\text{scalar}}$), have been deduced. We find that the contribution of exchange interaction to the anisotropic part of the relaxation rate ($k_{1\theta}$) is very small. Accordingly, we conclude that $k_{1\text{scalar}}$ is dominated by the intrinsic electron spin−lattice relaxation. From $k_{1\theta}$, a lower limit ($r > 10$ Å) has been deduced for the distance between the S-3 center and the *b*-heme.

Introduction

Succinate:ubiquinone oxidoreductase (SQR; complex II) links the oxidation of succinate to fumarate in the Kreb's cycle to the reduction of quinone to quinol in the respiratory chain in aerobic cells. The SQR from *Paracoccus denitrificans* contains four subunits, a flavoprotein (FP), an iron−sulfur protein (IP), and two hydrophobic polypeptides (QP).[1,16,17,25] The FP contains the dicarboxylate binding site and a covalently bound flavin moiety (FAD). Three iron−sulfur clusters, of type 2Fe-2S, 4Fe-4S, and 3Fe-4S, are part of the IP; these are often referred to as S-1, S-2, and S-3, respectively. Together, the FP and IP subunits constitute the succinate dehydrogenase (SDH) activity of the complex. In SQR, this soluble domain is anchored to the plasma membrane by the two hydrophobic polypeptides (QP). The QP binds one molecule of *b*-heme[26,32] and consists of two quinone binding sites.[32]

In the air-oxidized SQR, the S-3 center and *b*-heme are the only redox centers that are paramagnetic. Both centers are fully oxidized, as was determined in our earlier electron paramagnetic resonance (EPR) studies.[32] The S-3 center exhibits a prominent and almost isotropic EPR signal at $g = 2$, which may be used as an endogenous probe for the paramagnetic *b*-heme. Previous indirect evidence obtained on the bovine heart enzyme has pointed to the S-3 center being proximal to the *b*-heme.[25] Recently, we studied the electron spin relaxation properties of the S-3 center from *P. denitrificans* by cw EPR power saturation experiments.[32] Enhanced relaxation of S-3 was observed and taken as an evidence of the dipolar interaction between the S-3 and *b*-heme. An upper limit of the distance (r) between the S-3 and *b*-heme was inferred from the power saturation results ($r \leq 20$ Å).

This study is concerned with a more reliable estimate of the distance between the S-3 and *b*-heme in SQR. We exploit the effect of the dipolar and exchange interactions between the interacting spins and the dependence on electron spin−lattice relaxation rate of the more slowly relaxing S-3 center on these interactions to deduce the distance of the S-3 center from the neighboring *b*-heme.

Several methods have been used for measuring the electron spin−lattice relaxation. One is saturation recovery, in which a long saturating microwave pulse is applied to the entire spin system to drive it into a state away from equilibrium during the preparation period prior to observation of its recovery. This is the most widely used method, as this kind of measurement is not compromised by spectral diffusion in frozen solid, provided that the whole spectrum can be excited.[12] Electron spin−lattice relaxation rates are often determined by the inversion recovery method as well. Unfortunately, even for the most modern pulsed EPR instruments, the typical microwave field magnitudes are insufficient to saturate or invert the entire EPR spectrum of the S-3 center. As a result, the evolution of a perturbed EPR line toward equilibrium is driven by both the intrinsic spin−lattice relaxation process as well as the redistribution of the initial perturbation across the nonuniformly perturbed system.

In this paper, we implement the "picket-fence" pulse sequence in the inversion recovery experiment in order to exclude the

* To whom correspondence should be addressed. Telephone: (626)-395-6508. Fax: (626)-578-0471. E-mail: chans@its.caltech.edu.
[†] California Institute of Technology.
[‡] University of California.
[§] Present address: Health Economics Department, Bristol-Myers Squibb, Australia, 556 Princes Highway, Noble Park, VIC 3174, Australia.

10.1021/jp993693i CCC: $19.00
Published on Web 04/04/2000

influence of spectral diffusion on the observed recovery traces.[19] This pulse sequence allows us to obtain a more uniform initial perturbation[10,21] of the EPR spectrum of the S-3 center.

We find that, even under these conditions, the S-3 center exhibits spin−lattice relaxation behavior that deviates markedly from exponentiality. This is the result expected from the dipolar interaction between the S-3 center and the *b*-heme for a powder sample. Equations have been developed to describe the recovery traces of a "slow" relaxing spin when its spin−lattice relaxation is perturbed by pairwise interaction with a "fast" relaxing spin.[18,27] This treatment allows us to separate the orientation-dependent and isotropic contributions to the spin−lattice relaxation. We use this approach to obtain a more reliable estimate of the distance between the S-3 center and the *b*-heme in SQR.

Experimental Procedures

Materials. Triton X-100; poly(ethylene glycol) *tert*-octylphenyl ether; Tris(hydroxymethyl)aminomethane, Tris; and poly(oxyethylene) lauryl ether[30] were purchased from Boehringer Mannheim Corp., IN, or Mannheim, Germany. Centricon ultrafiltration tubes were from Amicon Inc., Beverly, MA; Sephadex G-50 was purchased from Sigma Chemical Co., St Louis, MO; Amberlite XAD-2 adsorbent was from Serva, Heidelberg, Germany. All other reagents were of AR grade.

Cell Growth, Enzyme Purification, and Analytical Procedures. Growth conditions for the strain PD1222/pPSD100 containing overproduced (∼2-fold) SQR and its construction have been described elsewhere.[24] SQR was purified by thawing the stored cell packs using 150−200 g of material each time. The purification procedure was as described previously,[26] with modifications similar to those described in refs 5 and 29. Prior to the EPR experiments, the enzyme was concentrated and the salt and Triton X-100 concentrations were reduced, the latter to ∼0.05% (w/v), by repeated exchange in Centricon 100 kDa cutoff concentrators against 100 mM Hepes, pH 7.4. The final yield was 1−2 mL of 50−100 μM SQR. The enzyme was considered to be sufficiently pure for use in our experiments according to two criteria: (i) optical spectra (negligible absorption from hemes other than b_{557}) and (ii) SDS−PAGE (>90%).[26] Enzyme concentrations were determined by measuring the acid-nonextractable FAD content of the samples.[33] Cytochrome *b* concentrations were determined from dithionite reduced-minus-oxidized difference spectra in a pyridine hemochrome assay mixture, using $\Delta\epsilon_{557-540} = 24.0\ \mathrm{mM}^{-1}\ \mathrm{cm}^{-1}$.[6] Typical [cytochrome *b*]/[FAD] ratios in our preparations were 1.3 ± 0.4. Samples stored at 193 K were thawed on ice before the pulsed EPR experiments. The concentration of SQR samples in the EPR experiments was ∼ 50 μM.

EPR Methods. The pulsed EPR experiments at X-band were conducted on a home-built instrument in the laboratory of Prof. R. D. Britt at UC−Davis.[31] The electron spin−lattice relaxation rates were measured with the picket-fence pulse sequence $\{\pi - \tau_{pf} - \pi - \tau_{pf} \ldots \pi - T - \pi/2 - \tau - \pi -$ ESE $\}$.[10,11] The pulse sequence was generated by a 0.1 ms clock. In this experiment, π pulses of ca. 20 ns were applied during a period of 0.1 ms and the interpulse times (τ_{pf}) between these π pulses are 1 μs. Echo intensity was monitored at time intervals T following the picket-fence pulses. The one picket pulse experiment is exactly equivalent to the standard inversion recovery experiment.[3,23] The interpulse time τ of 210 ns was used. The microwave power was 35 W at 9.26 GHz. The magnetic field was set at 3292 G (the resonance field corresponding to the absorption maximum of the signal of oxidized S-3).

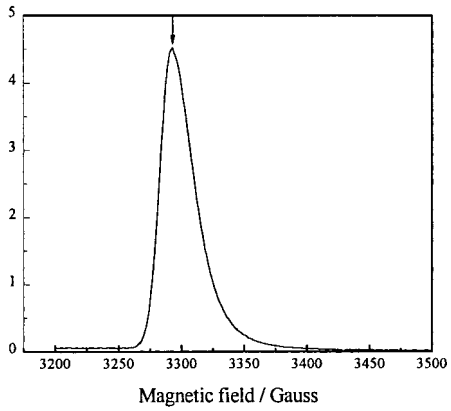

Figure 1. Field swept EPR absorption spectrum of air-oxidized SQR detected by spin−echo method with microwave frequency: 9.26 GHz. The spectral width of a 20 ns π pulse is approximately 18 G. The concentration of SQR in this sample is ∼50 μM.

In the picket-fence pulse sequence, many 180-degree pulses are sent in succession. Although spectral diffusion may compete with spin−lattice relaxation in filling in the hole created by an initial inversion pulse, in principle, with the application of many subsequent pulses, the entire spectral region in rapid spectral diffusional contact with the on-resonance bandwidth will be driven away from equilibrium, with only spin−lattice relaxation acting to drive the system back to the prepulse equilibrium. The result is a saturated spectrum from which the contribution of spectral diffusion to the spin−lattice relaxation is excluded.[4]

To measure T_2 of the *b*-heme, a two-pulse transverse relaxation experiment (sequence equivalent to two-pulse ESEEM) was performed. A $\pi/2 - \tau - \pi - \tau -$ echo sequence was used. The time for a $\pi/2$ pulse was 10 ns. Echo decays were recorded starting at 150 ns with 5 ns increment. Only data at 4.2 K were obtained due to the fast relaxing nature of the *b*-heme. The time constant for the ESE decay is referred to as T_m to encompass all processes that result in echo dephasing. The values obtained directly from these experiments are typically cited as the decay time constant. It is assumed that instantaneous diffusion makes a negligible contribution to the dephasing process, so T_m can be a reasonable estimate of T_2.

The temperature of the EPR sample was determined and controlled with a Lake Shore Cryotronics Model 805 temperature controller, which samples the resistance of a Lake Shore Cryotronics TG-120P gallium−aluminum−arsenide diode sensor mounted near the sample position of an X-band pulsed EPR probe inserted in the variable-temperature sample chamber of a Janis Supervaritemp liquid He cryostat. The system stabilizes the temperature at a set value by controlling the temperature of the cold He gas introduced into the sample chamber.[23]

Results

The field swept EPR spectrum of air-oxidized SQR (∼50 μM) at 4 K is shown in Figure 1. For the spin−lattice relaxation measurements, the magnetic field was set to the position marked by arrow (3292 G). This signal was characterized in our earlier work[32] as an isotropic signal arising from the oxidized S-3 center superimposed with a very weak and broad g_y component of the *b*-heme.[32]

Figure 2 presents examples of the inversion−recovery $[\pi - T - \pi/2 - \tau - \pi -$ ESE] transients observed at different temperatures. The recovery traces are clearly nonexponential. These inversion recoveries could be fitted to a sum of two exponentials, with decay constants equal to T_s and T_f, as

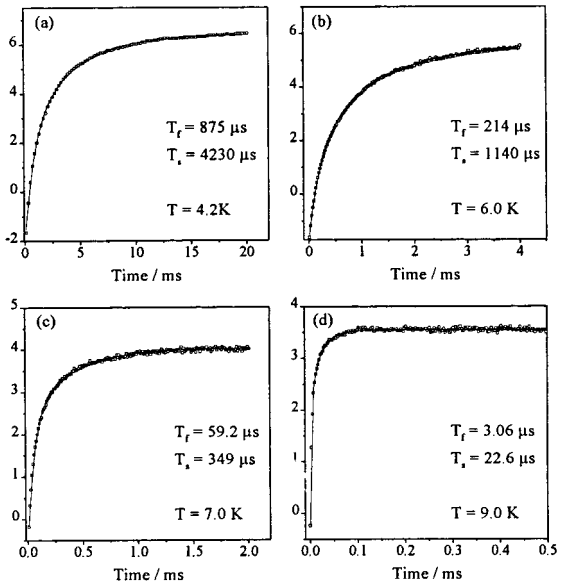

Figure 2. Inversion−recovery traces for the S-3 (3Fe−4S) center at different temperatures: (a) 4.2 K; (b) 6.0 K; (c) 7.0 K; (d) 9.0 K. The solid lines are obtained by fitting the data to a sum of two exponentials, and the two decay constants, T_f and T_s, are provided in each panel.

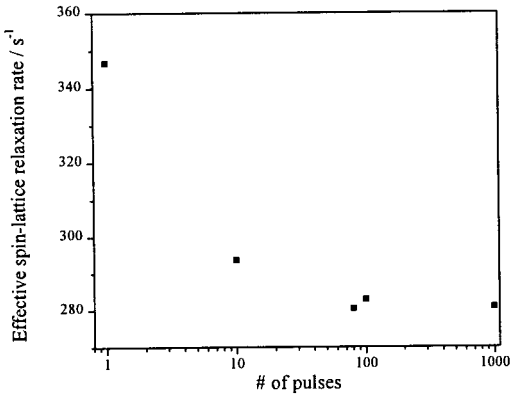

Figure 3. Dependence of the effective spin−lattice relaxation rate at 4 K for the S-3 center of SQR on the number of the picket-fence pulses.

highlighted for each panel. There are several possible reasons for this abnormal recovery behavior. First, the presence of a chemically distinct species at the same resonant field position could produce a biexponential recovery for this $g = 2$ signal.[32] However, magnetic dipolar interaction could also be the cause of this nonexponential behavior. Finally, this behavior could also arise from spectral diffusion. To eliminate the contribution of spectral diffusion to the relaxation transient, we have recorded the relaxation recovery using the picket-fence pulse sequence.

Elimination of Spectral Diffusion. The dependence of the effective electron spin−lattice relaxation rates for the S-3 center on the number of picket-fence pulses at 4 K is shown in Figure 3. Here the effective spin−lattice relaxation rate is measured by the time when the magnetization has decayed to 1/e of its initial value, assuming that the decay is exponential. Not surprisingly, this effective relaxation rate decreases with the number of picket-fence pulses and begins to level off as the number of picket-fence pulses is increased to 100. Thus, indeed, spectral diffusion is contributing to the original decay, but it can be effectively excluded by the use of the picket-fence pulse sequence. As a control, we have studied the relaxation of $CuSO_4$ in aqueous solution at 4 K using both inversion−recovery and picket-fence pulse sequences. A single-exponential decay of the

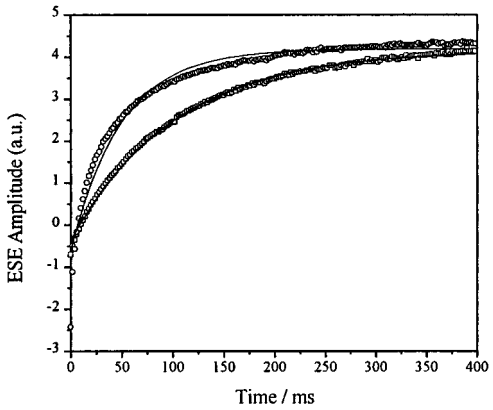

Figure 4. The picket-fence experiment of the Cu^{2+} ion (2 mM) at 4.2 K. One picket-fence pulse (inversion recovery) data (open circle) and data of 100 picket-fence pulse experiment (open rectangular) are superimposed with the single-exponential fits (solid line).

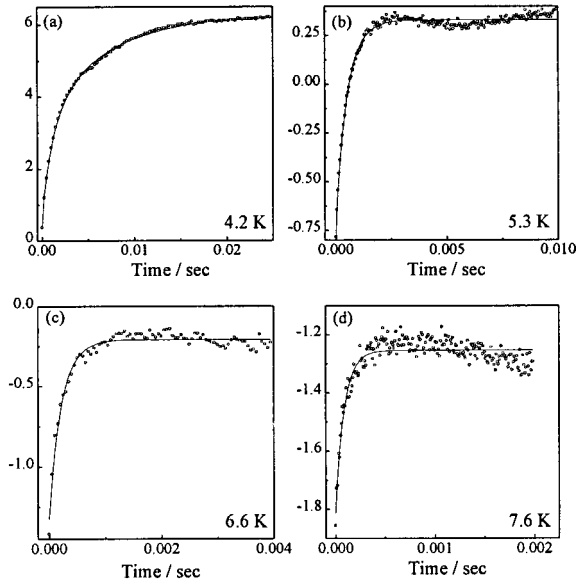

Figure 5. The recovery traces of the S-3 center (obtained by 100 picket-fence pulses) and the corresponding simulated curve using eq 13 at four different temperatures: (a) 4.2 K; (b) 5.3 K; (c) 6.6 K; (d) 7.6 K.

magnetization following elimination of spectral diffusion by the picket-fence sequence was observed (Figure 4). We have used $CuSO_4$ here as a control because Cu^{2+} is known to exhibit biexponential recovery due to spectral diffusion.

We have applied the picket-fence sequence (100 pulses) to record recovery traces of the S-3 center in SQR over a temperature range of 4−8 K and these data are shown in Figure 5 along with fits to the data as described below.

Anomalous Spin−Lattice Relaxation of the S-3 Center. We found that the recovery trace remains nonexponential at 4 K (Figure 6), even after the spectral diffusion effect is excluded by use of the picket-fence sequence. We surmise that this nonexponential recovery arises either from spectral interference from an overlapping signal or from dipolar interaction with another magnetic center that is relaxing rapidly.

If the nonexponential behavior is caused by the superposition of the S-3 signal and the signal of *b*-heme at $g = 2$ ($g_y^{b-\text{heme}} = 2.1$),[32] presumably a biexponential model can be used to describe it. The recovery trace is fitted by a biexponential in Figure 6 and the fitting parameters are shown in Table 1. As reported in our previous study,[32] the *b*-heme has a very broad and weak signal at $g_y = 2.1$ and a small signal at $g_z = 3.6$ (at least 200

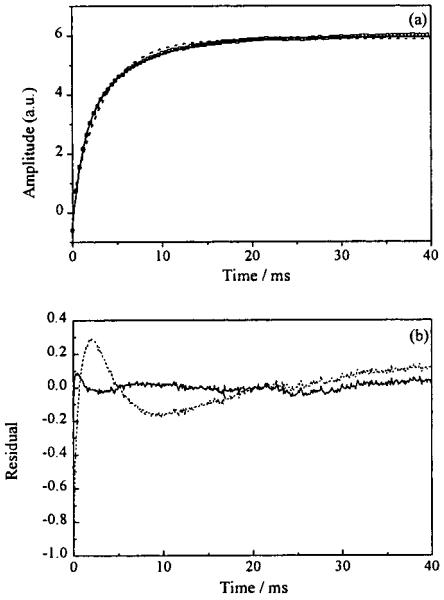

Figure 6. (a) The picket-fence data of the S-3 center at 4.2 K (open circle) obtained by 1000 π pulses superimposed with single-exponential (dashed line) and biexponential (solid line) fits. (b) The residual of single-exponential (dashed line) and biexponential (solid line) fit.

TABLE 1: Time Constants and Fitting Coefficients for the Recovery Traces of the S-3 Center at 4 K Using the Biexponential[a] and Single-Exponential[b] Models[c]

#	biexponential					single exponential	
pulses	T_f (ms)	T_s (ms)	C_f	C_s	R^2	T_1 (ms)	R^2
1	0.7298	4.4704	3.4046	4.8365	0.99939	2.8847	0.98547
10	1.1178	5.2910	2.8166	3.2455	0.99927	3.4058	0.98756
80	0.8674	6.9325	2.9489	3.3616	0.99907	3.5667	0.97503
100	1.4941	6.3189	3.4360	2.8257	0.99937	3.5347	0.98782
1000	1.2534	5.9431	3.2079	3.1731	0.99940	3.5604	0.98619

[a] Mo − $C_f \exp(-t/T_f) - C_s \exp(-t/T_s)$. [b] Mo − $C \exp(-t/T_1)$. [c] M_0, C_f, C_s, and C are fitting parameters; T_f and T_s are the fast and slow relaxation time constants, respectively; T_1 is the effective spin−lattice relaxation time constant.

times smaller in magnitude than the S-3 signal). It is also expected to have a faster relaxation rate compared to the S-3 center. However, as shown in Table 1, the difference between the faster relaxation rate (T_f) and slower relaxation rate (T_s) constants is within 1 order of magnitude. Also, the signal intensity of the *b*-heme is much smaller than that of the S-3 center.[32] The weights (C_f and C_s in Table 1) of these two relaxation rates are expected to be very different, but they are not. Therefore, we have excluded the possibility of a significant *b*-heme contribution to the inversion recovery.

Instead, we have attributed the anomalous relaxation behavior of the S-3 center to a tensor magnetic dipolar interaction between the S-3 center and the low-spin *b*-heme. This interaction produces a "powder" distribution of spin−lattice relaxation rates, and thus the composite decay should not be exponential. A similar nonexponential recovery is apparently not observed for the magnetically isolated 3Fe-4S cluster in fumarate reductase (FRD), the homologue enzyme that catalyzes the reverse reaction. The FRD does not contain the *b*-heme. Shergill et al.[28] have studied the spin−lattice relaxation of the oxidized 3Fe-4S in FRD at 10 K using the inversion recovery pulse sequence and have interpreted the data in terms of a single exponential.

Analysis of the Relaxation Recovery. In the air-oxidized state of SQR, only the S-3 center and the *b*-heme are paramagnetic. The *b*-heme is a low-spin ferric center with S = $^1/_2$. In the case of the [3Fe-4S] cluster, antiferromagnetic exchange among the three ferric ions also leads to a S = $^1/_2$ ground state with near isotropic *g* values ($g \sim 2.0$).[15] Accordingly, we can treat this system as an isolated pair of electron spins separated by a fixed distance (*r*). The two spins, however, differ in their relaxation properties: the *b*-heme is rapidly relaxing, whereas the S-3 center is slowly relaxing. If the two spins are in close proximity, as appears to be the case here, then the rapidly relaxing *b*-heme can influence the relaxation of the slow-relaxing S-3 center. Specifically, the spin−lattice and transverse relaxation rates of the "slow"-relaxing spin can be affected by scalar exchange coupling and tensor magnetic dipolar interaction between the "fast" and "slow" relaxing spins. The spin−lattice relaxation of the "slow" relaxing spin will then include three contributions: intrinsic relaxation, scalar exchange coupling, and the tensor magnetic dipolar interaction. The intrinsic and the scalar exchange relaxation rates are isotropic, and together they contribute a single-exponential rate constant to the spin−lattice relaxation transients. However, the dipolar relaxation rate is orientation dependent.

Accordingly, the observed rates of spin−lattice relaxation can be described by

$$k_{1obs}(\theta) = k_{1scalar} + k_{1\theta} \tag{1}$$

where $k_{1scalar} = k_{1i} + k_{1ex}$. Here, k_{1i} is the intrinsic spin−lattice relaxation rate, k_{1ex} is the contribution to the relaxation rate due to superexchange, and $k_{1\theta}$ denotes the dipolar relaxation rate previously derived by Kulikov and Likhtenstein[22] and by Goodman and Leigh[14] as well as cross-relaxation terms arising from superexchange and magnetic dipolar interaction (see Appendix I and II for details). For a given orientation θ of the interspin vector with respect to the applied magnetic field

$$k_{1\theta} = (B + C + E) \tag{2}$$

The corresponding contribution to T_2 is

$$k_{2\theta} = \left(A + \frac{1}{2}B + \frac{C}{2} + 2D + \frac{E}{2}\right) \tag{3}$$

The terms $A-E$ are given by

$$A = \frac{1}{3}T_{1f}\left[J^A\sqrt{S(S+1)} + \frac{\gamma_s\mu_f}{r^3}(1 - 3\cos^2\theta)\right]^2 \tag{4}$$

$$B = \left(\frac{8}{3}\right)\frac{T_{2f}}{1 + (\omega_s - \omega_f)^2T_{2f}^2}\left[\frac{J^B\sqrt{S(S+1)}}{2} + \frac{\gamma_s\mu_f}{4r^3}(1 - 3\cos^2\theta)\right]^2 \tag{5}$$

$$C = \frac{3T_{1f}}{1 + \omega_s^2\,T_{1f}^2}\left[J^C\sqrt{S(S+1)} + \frac{\gamma_s\mu_f}{r^3}\sin\theta\cos\theta\right]^2 \tag{6}$$

$$D = \left(\frac{3}{2}\right)\frac{T_{2f}}{1 + \omega_f^2\,T_{2f}^2}\left[J^D\sqrt{S(S+1)} + \frac{\gamma_s\mu_f}{r^3}\sin\theta\cos\theta\right]^2 \tag{7}$$

$$E = \left(\frac{3}{2}\right)\frac{T_{2f}}{1 + (\omega_s + \omega_f)^2T_{2f}^2}\left[\frac{J^E\sqrt{S(S+1)}}{2} + \frac{\gamma_s\mu_f}{r^3}\sin^2\theta\right]^2 \tag{8}$$

where γ_s is the magnetogyric ratio for the slow spin; μ_f is the magnetic dipole moment of the fast relaxing spin; *r* is the

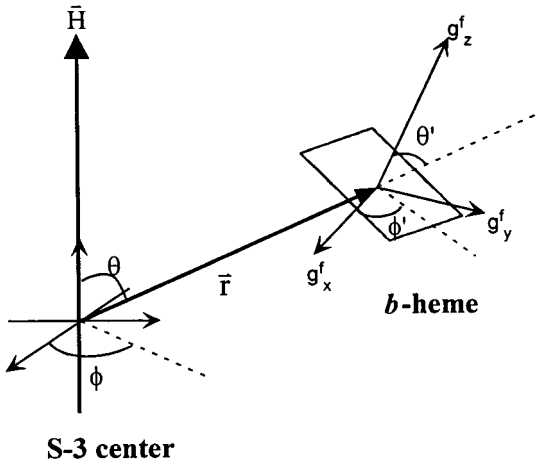

Figure 7. Relationship between the coordinate systems of the magnetic field, the interspin vector, and the *g*-tensor of *b*-heme. The orientation of the interspin vector with respect to the magnetic field: θ and ϕ. The orientation of $\tilde{g}$ tensor principal axes of *b*-heme with respect to the interspin vector: θ' and ϕ'.

interspin distance; J^A, J^B, J^C, J^D, and J^E denote the exchange contributions arising from the scalar and anisotropic electron exchange between the S-3 center and *b*-heme (Appendix II); T_{1f} and T_{2f} are the spin−lattice and transverse relaxation times of the fast relaxing spin; and ω_s and ω_f are the Larmor frequencies of the slow (observed) and fast spins, respectively. These expressions are valid when T_{1f} and $T_{2f} \ll T_{1s}$, the conditions observed here.

From these expressions, it is evident that $k_{1\theta}$ and $k_{2\theta}$ are dependent on the orientation of the interspin vector with respect to the applied magnetic field. For any one orientation of the interspin vector (θ, ϕ), the inversion recovery will decay exponentially with decay constant $k_1(\theta)$. Aside from r, T_{1f}, T_{2f}, and J^B, $k_{1\theta}$ also depends on ω_s and ω_f. In our experiments, the slow spin (S-3 center) resonates over a wide range of frequency (100 G) while a 20 ns pulse has only a spectral width of ∼18 G. Therefore, the pulse is not able to excite the whole envelope of the S-3 center absorption. However, the signal of the S-3 center is approximately isotropic, so ω_s can be regarded as a constant for all orientations. On the other hand, the fast relaxing *b*-heme in SQR has a rhombic EPR signal, so that its Larmor frequency, ω_f, varies with the orientation of the protein molecule with respect to the applied magnetic field (see Appendix I for detail). For a given orientation (θ, ϕ) of the interspin vector relative to the applied magnetic field (Figure 7)

$$\mu_f = g_f(\theta, \phi)\beta[S(S+1)]^{1/2} = \frac{\sqrt{3}}{2}\beta g_f(\theta, \phi) \qquad (9)$$

and

$$\omega_f = g_f(\theta, \phi)\beta H_0 \qquad (10)$$

Here. $g_f(\theta, \phi)$ in turn depends on the orientation of the $\tilde{g}$ tensor of the *b*-heme vis a vis the magnetic field. Specifically,

$$g_f(\theta, \phi) = (g_z^{f2}\cos^2\eta + g_x^{f2}\sin^2\eta\cos^2\epsilon + g_y^{f2}\sin^2\eta\sin^2\epsilon)^{1/2} \qquad (11)$$

where g^f_x, g^f_y, g^f_z refer to the principal components of the $\tilde{g}$ tensor for the *b*-heme, and (η, ϵ) denote the polar and azimuthal angles of the applied magnetic field vis a vis these principal axes. The detailed relationship between the effective $g_f{}^{b-\text{heme}}$ (θ, ϕ), or $g_{\text{eff}}{}^{b-\text{heme}}$ (θ, ϕ), and the orientations of the *b*-heme (θ', ϕ') vis a vis the interspin vector is given in Appendix I. Two sets of the angles, (θ, ϕ) and (θ', ϕ'), between these three coordination systems, the $\tilde{g}$ tensor of the *b*-heme, the interspin vector, and the magnetic field are shown in Figure 7.

Due to the distribution of orientations (θ, ϕ) within the sample, the observed recovery traces will be the sum of exponentials. For a uniform distribution of interspin vectors, we can write

$$\frac{I(t)}{I(0)} = 1 - \frac{1}{4\pi}\int_0^{2\pi}\int_0^{\pi} e^{-(k_{1\text{scalar}}+k_{1\theta})t}\sin\theta\, d\theta d\phi \qquad (12)$$

where $I(t)$ is the intensity of the recovery transient at time t and $I(0)$ is the initial intensity. Since the EPR signal of the S-3 center has no evident splitting caused by the exchange interaction with the *b*-heme, we suspect that the values of J are very small. We then will fit the data in the limit of J^A, J^B, J^C, J^D, and $J^E \rightarrow 0$ (for nonzero J^A, J^B values see below). Furthermore, to reach the limit $(\omega_s - \omega_f)^2\, T_{2f}{}^2 \gg 1$, it requires $T_{2f} \gg 0.01$ ns at X-band. This is a reasonable range of T_{2f} ($0.001 < T_{2f} < 1\ \mu$s) for a first row transition metal below liquid nitrogen temperature. Therefore, eq 12 simplifies to

$$\frac{I(t)}{I(0)} = 1 - e^{-k_{1\text{scalar}}t}\frac{1}{4\pi}\int_0^{2\pi}\int_0^{\pi}(e^{-k_{1d}\mu_f{}^2(\mathbf{b}+\mathbf{c}+\mathbf{e})t})\sin\theta d\theta d\phi \qquad (13)$$

where we have defined $k_{1d} = \gamma_s^2/r^6$.

The terms **b**, **c**, **e** are

$$\mathbf{b} = \frac{(1-3\cos^2\theta)^2}{6(\omega_s - \omega_f(\theta,\phi))^2 T_{2f}} \quad \mathbf{c} = \frac{3\sin^2\theta\cos^2\theta}{\omega_s^2 T_{1f}}$$

$$\mathbf{e} = \frac{3\sin^4\theta}{2(\omega_s + \omega_f(\theta,\phi))^2 T_{2f}} \qquad (14)$$

Of the three terms in eq 13, the last term, i.e., the **e** term, is usually unimportant. Hirsh and Brudvig[18] have shown that either the **b** or **c** term dominates $k_{1\theta}$ for isotropic spin systems.

Investigation on the Relative Contributions of b, c, and e Terms in Equation 13. Equation 12 was integrated over θ and ϕ at specific orientations (θ', ϕ') of the *b*-heme with respect to the interspin vector (Figure 7). We used g^f_x, g^f_y, and g^f_z of 1.5, 2.1, and 3.6, respectively, for the *b*-heme. For SQR, there is a defined orientation of the interspin vector relative to the principal axes of the *b*-heme $\tilde{g}$ tensor. Unfortunately, in the absence of a structure for SQR, this orientation (θ', ϕ') is not known (Figure 7). Accordingly, we have examined various possibilities of this orientation, and the effects of this orientation on the relative contributions of the **b**, **c**, **e** terms in $k_{1\theta}$ (see Appendix III for detail). The **b**, **c**, and **e** term contributions are summarized in Figures 14−16. There, the **b**, **c**, **e** terms are plotted as a function of ϕ for various θs for three combinations of θ' and ϕ' (Figure 14 for $\theta' = \phi' = 0°$; Figure 15 for $\theta' = 30°$, $\phi' = 0°$; and Figure 16 for $\theta' = 90°$, $\phi' = 0°$) and assuming $T_{1f} = T_{2f} = 0.1\ \mu$s (see discussion and ref 27). Although the **b** term will not dominate when $(1 - 3\cos^2\theta)^2/6 < 3\sin^2\theta\cos^2\theta$, a condition that is obtained for $\theta = 40°\sim 60°$ and $120°\sim140°$, when eq 13 is integrated over θ and ϕ, the **b** term dominates.

We reach the same conclusions if we ignore the variation of g_f/g_s in eq 14, i.e., if we assume that *b*-heme $\tilde{g}$ tensor is isotropic and g_f is set equal to the average value of 2.2. In this limit, the three terms depend only on angle θ (see eq 14). Figure 8 shows the comparison of the magnitude of these three terms assuming $T_{1f} = T_{2f} = 0.1\ \mu$s. Again, it is evident that the **b** term dominates

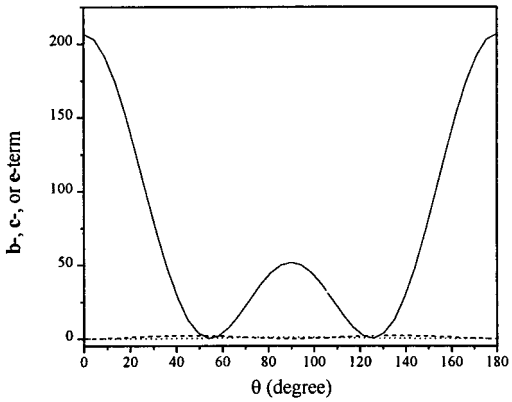

Figure 8. Comparison of the magnitude of **b**, **c**, and **e** terms of eq 14. **b** (solid line), **c** (dashed line), and **e** term (dotted line). Values are plotted versus θ. $T_{1f} = T_{2f} = 10^{-7}$ sec, and g_f (*b*-heme) fixed at 2.2.

the other two terms, except when $(1 - 3\cos^2\theta) \approx 0$, or for θ near 54.74° or 125.26°, where all three terms are equally small. The same behavior was observed if $T_{1f} = T_{2f} = 0.01$ μs was used in calculation (data not shown).

From these results, it is evident that the **b** term is the only dominant one for essentially any orientation of the *b*-heme tensor axes relative to the interspin vector. Apparently, $\omega_s - \omega_f \ll \omega_s$ or $\omega_s + \omega_f$ for any orientation of the *b*-heme. Moreover, T_{2f} is typically shorter than T_{1f}, and we have taken $T_{1f} = T_{2f}$ in these sample calculations in order to deaccentuate the contribution of **b** and **c** terms as much as possible. Therefore, we may conclude with a high degree of assurance that the magnetic dipolar contribution to $k_{1\theta}$ comes principally from the **b** term only, for any orientation of the *b*-heme relative to the interspin vector.

Simulations of the Magnetization Recovery. Simulations of the magnetization recovery were obtained at 4 K using the **b** term with $J^B = 0$ (eq 13) for various orientations of the *b*-heme (θ', ϕ') relative to the interspin vector. (θ' is the angle between the interspin vector and *z* axis of the $\tilde{g}$ tensor for the *b*-heme; ϕ' is the angle between the interspin vector and *x* axis.) The distance between the S-3 center and *b*-heme is included in k_{1d}. In the absence of a reliable T_{2f} measurement of the *b*-heme, we fit the data to yield $T_{2f}{\cdot}r^6$.

The simulation parameters that gave good fits are summarized in Table 2. From these results, we see that $k_{1scalar}$ ranges from 100 to 170 s^{-1} depending on the orientation (θ', ϕ') assumed and used to simulate the recovery. The $T_{2f}{\cdot}r^6$ distance obtained for the different heme orientations varies between $0.16 \sim 0.50$ μs·nm^6. A plot illustrating the relationship between T_{2f} and r for this range of $T_{2f}{\cdot}r^6$ as well as for $T_{2f}{\cdot}r^6 \sim 0.26$ is shown in Figure 9.

Two-Pulse Transverse Relaxation Measurement of the *b*-Heme. To have a good estimate of interspin distance between the S-3 center and *b*-heme, T_{2f} for the *b*-heme is needed. As noted in our previous study on SQR, the *b*-heme signal at $g = 3.6$ is very weak. The low intensity of the *b*-heme need not be associated with an unusually short T_1 or T_2. In derivative spectrum, the dispersion of the signal near g_z might be more important in determining the appearance of the signal than relaxation factors. We have undertaken two-pulse spin−echo measurement of this signal at 4.2 K in an attempt to deduce the transverse relaxation time of the *b*-heme (T_{2f}). From the two-pulse spin−echo decay, T_m was the relaxation time constant obtained by fitting the data using a single-exponential decay (Figure 10). In addition to exponential decay, modulations are also shown in Figure 10, but we focus on the decay caused by transverse relaxation here. However, it should be noted that the

TABLE 2: Simulation Parameters of the Recovery Trace of the S-3 Center at 4 K (Figure 5a) for Various Heme Orientations Relative to the Interspin Vector

(θ', ϕ')	$k_{1scalar}$ (s^{-1})	$T_{2f}{\cdot}r^6$ (μs·nm^6)	(θ', ϕ')	$k_{1scalar}$ (s^{-1})	$T_{2f}{\cdot}r^6$ (μs·nm^6)
0°, 0°	112.1	0.22	20°, 70°	106.1	0.24
0°, 30°	109.7	0.21	20°, 80°	104.7	0.23
0°, 60°	114.6	0.22	20°, 90°	103.3	0.21
0°, 90°	113.9	0.23	30°, 0°	148.6	0.36
10°, 10°	106.8	0.20	30°, 30°	123.0	0.30
10°, 20°	103.7	0.18	30°, 40°	131.5	0.29
10°, 30°	107.1	0.20	30°, 60°	130.5	0.32
10°, 40°	104.3	0.19	30°, 90°	89.32	0.23
10°, 50°	104.1	0.18	60°, 0°	129.5	0.25
10°, 60°	104.9	0.20	60°, 20°	121.2	0.26
10°, 70°	112.4	0.23	60°, 40°	152.9	0.34
10°, 80°	118.0	0.25	60°, 60°	152.6	0.31
10°, 90°	106.6	0.20	60°, 90°	124.1	0.22
20°, 0°	124.6	0.24	90°, 0°	129.5	0.40
20°, 10°	126.8	0.26	90°, 10°	151.2	0.37
20°, 20°	141.9	0.31	90°, 20°	171.2	0.50
20°, 30°	130.9	0.26	90°, 45°	136.0	0.16
20°, 40°	117.9	0.24	90°, 60°	169.1	0.35
20°, 50°	105.5	0.21	90°, 80°	146.7	0.29
20°, 60°	106.4	0.20	90°, 90°	130.5	0.19

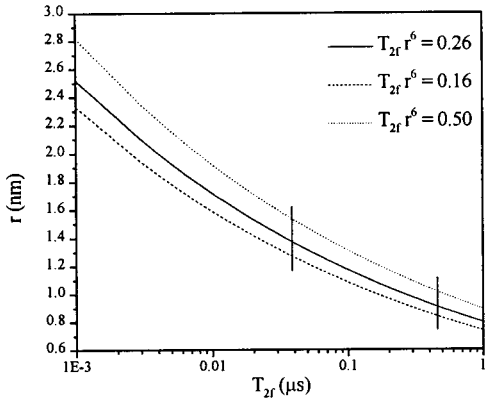

Figure 9. The relationship of r versus T_{2f} generated by the $T_{2f}{\cdot}r^6$ obtained from the simulations. $T_{2f}{\cdot}r^6 = 0.26$ μs·nm^6 (solid line), $T_{2f}{\cdot}r^6 = 0.16$ μs·nm^6 (dashed line), and $T_{2f}{\cdot}r^6 = 0.50$ μs·nm^6 (dotted line). The vertical line at the right marks the T_{2f} obtained from the two-pulse spin−echo experiment and the vertical line at the left marks the lowest T_{2f} observed for low-spin hemes.

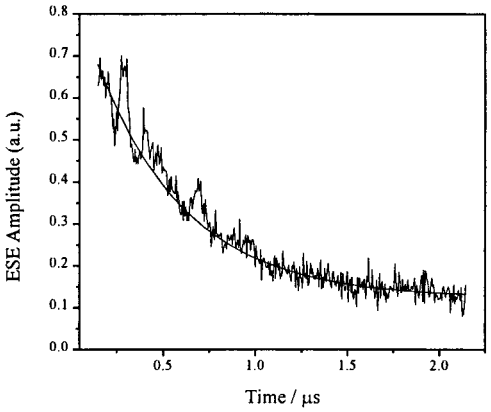

Figure 10. Two-pulse spin−echo decay of the *b*-heme of SQR measured at $g = 3.04$ (microwave frequency: 10.22 GHz, magnetic field: 2402 G) superimposed with single-exponential fit.

T_m measured here can only be an upper limit to the real T_2, since it is possible that certain components of the heterogeneous signal are missed in the two-pulse experiments. Thus, we have $T_{2f} \leq T_m = 0.48$ μs, and we obtain a lower limit to r of 9 Å from the limiting range of $T_{2f}{\cdot}r^6$ ($8.33 < r < 10.07$ Å).

TABLE 3: Simulation Parameters with the Addition of Exchange Interaction (other parameters as the simulations in Table 2)

(θ', ϕ')	k_{1i} (s^{-1})	r (Å)	J^B (MHz)
0°, 0°	119.4	9.46	1.2
90°, 0°	127.6	10.6	3.54
0°, 90°	129.7	9.70	1.55
90°, 90°	147.1	10.8	6.01
45°, 0°	129.6	9.71	2.34
0°, 45°	128.2	9.66	2.13
60°, 60°	133.7	9.48	2.54
30°, 30°	119.7	9.78	2.98
0°, 30°	126.4	9.62	2.48
30°, 0°	143.8	10.0	3.10
60°, 0°	120.8	9.44	2.77
0°, 60°	128.1	9.64	1.83
45°, 45°	135.7	9.82	1.91

TABLE 4: Simulation Parameters for the Recovery Traces of the S-3 Center Measured at Different Temperatures (Figure 5)

temp (K)	$k_{1scalar}$ (s^{-1}) (case A)	$k_{1scalar}$ (s^{-1}) (case B)
4.2	105.52	105.52
5.3	1562.0	1111.2
6.6	3953.7	2094.5
7.6	10252	6064.8

Contribution of the Exchange Interaction between the S-3 Center and the *b*-Heme. It should be noted that the exchange interaction (**S·J·S**) becomes important when the distance between spins is less than a few Å (~10 Å). The exchange interaction contributes to the same $S_{1\pm}S_{2\mp}$ matrix elements of the dipole−dipole interaction Hamiltonian that are the basis of the *B* term (Appendix II). The addition of nonzero values of J^B was tested to determine if the fit to the data could be improved. Again, these simulations (Table 3) were examined for different heme orientations (θ', ϕ'). The fits to the data were not significantly improved with the addition of the exchange interaction. In any case, the exchange interaction required to improve the fits is small (≤6 MHz).

Temperature Dependence of the Relaxation Time Constants. The recovery traces remain nonexponential over a temperature range of 4−8 K. At higher temperatures, we were not able to obtain data with sufficient signal-to-noise ratio because the S-3 center relaxes very fast. We simulated the data measured at the higher temperatures (data not shown) by fixing the value of T_{2f}•r^6 to the average value estimated from the data obtained at 4.2 K; that is, $k_{1\theta}$ was assumed to be independent of temperature and $k_{1scalar}$ was treated as the only adjustable parameter in simulations ($k_{1\theta}$ is a function of T_{2f}, θ, ϕ, θ', ϕ', and r^6 when only the **b** term is considered). This approximation assumes that T_{2f} is independent of temperature (case A), which is of course not correct.

Since $k_{1\theta}$ is proportional to $1/T_{2f}$ and $k_{1scalar}$ is related to the intrinsic $1/T_{1s}$, the temperature dependence of $k_{1scalar}$ should dominate the observed overall spin−lattice relaxation rate. Typically, T_2 exhibits a smaller temperature dependence compared to T_1. For example, in the low-spin ferric porphyrin, the temperature dependence of T_2 is much smaller than that of T_1.[27] For an upper limit on the temperature dependence of T_{2f} (case B), we scaled T_{2f} by the temperature dependence of $k_{1scalar}$. The calculated recovery curves for the S-3 center signal at four temperatures are shown in Figure 5. The values of simulation parameters used to simulate the curves for the two limits are given in Table 4. Figure 11 depicts the temperature dependence of the rate constant $k_{1scalar}$ for the S-3 center for the two limiting cases. As expected, $k_{1scalar}$ increases with increasing temperatures. As noted earlier, $k_{1scalar}$ consists of two parts; k_{1i} and k_{1ex}. Since the exchange contribution is small, i.e., J^B is small, $k_{1scalar}$ is dominated by k_{1i}.

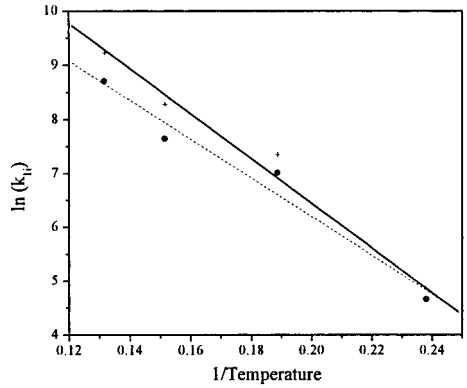

Figure 11. The temperature dependence of the spin−lattice relaxation rate for S-3. The solid line is the fit of the data (case A: +) to exp(−41.6/*T*) for an Orbach process. The dashed line is the fit of the data (case B: •) to exp(−36.0/*T*).

Discussion

In a previous inversion recovery study of the S-3 center in fumarate reductase, the observed magnetization recovery was interpreted in terms of a simple exponential.[28] Only the 3Fe−4S center was paramagnetic in this previous study. In our present study on SQR, we have observed nonexponential behavior of the S-3 center, and have shown that the magnetization recovery following inversion remains nonexponential, even after spectral diffusion effects are excluded by use of the picket-fence sequence. Since in SQR, the oxidized S-3 center coexists with the oxidized *b*-heme for the protein as isolated, we have attributed the anomalous spin−lattice relaxation of the S-3 center to magnetic tensor dipolar interaction and electron exchange interaction between the 3Fe−4S cluster and the *b*-heme. A theoretical model based on these interactions has been developed to account for the observed nonexponential decays, and recovery traces were simulated under varying conditions for comparison with experiment.

As expected, the contribution of the dipolar interaction to the relaxation of the S-3 center depends on the orientation of the *b*-heme relative to the vector between the interacting magnetic centers. In the absence of a structure for SQR, this orientation is, of course, not known. However, from the simulations of the 4 K data, we were able to obtain a range of possible value for T_{2r}•r,[6] depending on the orientation of the *b*-heme.

Based on the two-pulse spin−echo experiment of the *b*-heme, we have estimated a $T_{2f} = 0.48$ μs for the heme. From plots of r versus T_{2f} in Figure 9, the distance r could be determined to be in the range of 8.3−10.1 Å (right vertical line in the figure). Since the two-pulse spin−echo experiment provided merely an upper limit for T_{2f}, we conclude that this analysis offers a lower limit of 9 Å to the distance between the interacting centers.

On the other hand, a lower limit to T_{2f} could be inferred from the spin−lattice relaxation and transverse relaxation rates of known low-spin hemes. Eaton and co-workers[27] have examined the transverse relaxation rate for a number of low-spin iron porphyrins between 10 and 25 K. The T_2's of these centers are around 0.1~1.0 μs (0.21~0.63 μs) over this temperature range; thus, the rates are only weakly temperature dependent. Our two-pulse spin−echo measurement of the *b*-heme also yielded a T_{2f} that fell within this reasonable range. For other low-spin hemes, $T_2 \approx 0.13$ μs for cyt. *c* at 10 K[2,9] and 0.036 μs for the cyt. *a* in

cytochrome *c* oxidase at 15 K.[14] Note that these T_{2f}'s also fit the limit set before (eq 13), i.e., $T_{2f} \gg 0.01$ ns. If we take 0.036 μs as the lower limit of T_{2f} for the *b*-heme in SQR, an upper limit of 12.7∼15.4 Å can be obtained for *r* (left vertical line in Figure 9).

The above conclusions were based on an analysis that assumed only magnetic tensor dipolar interaction between the S-3 center and the *b*-heme. However, the exchange interaction (**S**·**J**·**S**) becomes important when the distance between the interacting spins becomes sufficiently short, say, ≈ 10 Å. Since $r \geq 10$ Å in the present problem, the exchange interaction to the relaxation is expected to be small. The addition of an exchange contribution (J^B) did not significantly improve the fits. Nevertheless, the possibility of a small contribution from the electron exchange interaction ($J^B \leq 6$ MHz) cannot be excluded.

Although a constant value of J^B was used in these simulations to include the effect of electron exchange, strictly speaking the exchange contribution J^B to the *B* term is also angle dependent. The presence of a low-spin heme species allows for anisotropic components in the exchange interaction due to the low-lying orbital states, in addition to those from the dipolar term. As shown in Appendix II, anisotropic exchange would contribute to an effective interaction that is dependent on the orientation of the interacting spin system vis a vis the applied magnetic field. However, since only the "*B* term" contributes to the nonexponential behavior in the T_1 decay of the S-3 center, there is no way to distinguish between isotropic versus anisotropic exchange contributions arising from the interaction of S-3 center with the *b*-heme. Moreover, when the exchange interaction is weak and is not even detected as a scalar interaction, its orientation dependence will escape detection as well.

We therefore conclude that the $k_{1\theta}$ is dominated by the magnetic dipole−dipole interaction. If so, the exchange interaction can contribute only in a minor way to the scalar relaxation rate. That is, $k_{1scalar}$ is dominated by k_{1i}.

Gayda et al.[13] and Bertrand et al.[7] have reported T_1 for the 3Fe−4S center in ferredoxin II *from Desulfovibrio gigas* and ferredoxin I from *Azotobacter vinelandii* at low temperatures (4−10 K) using the power saturation method. These authors obtained $1/T_1$ values on the order of 1000 s^{-1} near 4 K, which is close to, but larger than, the $1/T_1$ deduced from our measured values of $k_{1scalar}$. From this correspondence, we surmise that the contribution from exchange interaction between the S-3 center and the *b*-heme to $k_{1scalar}$ could not be significant in SQR, in accord with our present conclusions.

In addition, the earlier results on the ferredoxins demonstrated that the relaxation behavior of the isolated 3Fe−4S cluster in these ferredoxins could be adequately described by the Orbach process, and their temperature dependences were used to deduce the energy of the lowest excited level in each of these clusters. An energy of about 20 cm^{-1} was obtained for both clusters. For the S-3 center in SQR, the temperature dependence of $k_{1scalar}$ ($\approx k_{1i}$) gave a simple exponential dependence [exp(−41.6/*T*) and exp(−36.0/*T*) for case A and case B, respectively], clearly suggesting an Orbach mechanism for the intrinsic relaxation of the 3Fe−4S cluster as well. From the data, we obtained energies of 29 ± 3.1 cm^{-1} and 25 ± 3.2 cm^{-1} for the two limiting cases.

For short interspin distances, one might expect splittings of the S-3 EPR signal by the exchange coupling. In the present instance, the magnitude of J^B is clearly small (<6 MHz), and any splitting would be limited by the line width of the S-3 signal.

The role of the two redox centers, 4Fe−4S cluster (S-2 center) and *b*-heme, in the electron transfer pathway of SQR has been puzzling because of their low reduction potentials. In the recently solved X-ray crystal structure of fumarate reductase,[20] the iron−sulfur clusters are arranged in the sequence 2Fe−2S···4Fe−4S···3Fe−4S (S-1···S-2···S-3), and each of them are 13∼14 Å apart. Involvement of the S-2 center in the electron transfer pathway was suggested on the basis of these results.[20] However, unlike SQR there is no heme in FRD. We speculate that the *b*-heme could mediate the electron transfer from the S-3 center to the quinone in SQR. The distance between the *b*-heme and the S-3 center deduced here is within the range of common cofactor separation distance observed in multicentered electron transfer proteins. However, the detailed mechanism of involvement of the *b*-heme in shuttling electrons or reducing equivalents to the quinone remains to be established.

Conclusions

The interspin distance between the S-3 center and *b*-heme in SQR has been estimated by simulating the recovery traces of the S-3 center measured by picket-fence pulse sequence. A lower limit of 10 Å was obtained. The temperature dependence of the intrinsic spin−lattice relaxation rate of the S-3 center suggests an Orbach mechanism for the process.

Acknowledgment. We thank Dr. Brian E. Schultz and Professor Gary W. Brudvig for numerous discussion on this work. This work was supported by the NIH grants GM22432 (to S.I.C.) and GM48242 (to R.D.B.) from the U.S. Public Health Service.

Appendix I

We defined the interspin vector as **X**(*x*, *y*, *z*) coordinate. The angles between the interspin vector and the magnetic field are θ and ϕ. The unit vector along the magnetic field can be expressed in this coordinate as

$$\hat{n} = \sin\theta\cos\phi\,\hat{x} + \sin\theta\sin\phi\,\hat{y} + \cos\theta\,\hat{z} \qquad \text{(A1)}$$

The **X**′(*x*′, *y*′, *z*′) coordinate of *b*-heme *g*-tensor can be defined by the two angles between the **X** and **X**′ coordinate, θ' and ϕ'.

$$\mathbf{X}' = \mathbf{A}\mathbf{X} = \begin{pmatrix} \cos\theta'\cos\phi' & \cos\theta'\sin\phi' & -\sin\theta' \\ -\sin\phi' & \cos\phi' & 0 \\ \sin\theta'\cos\phi' & \sin\theta'\sin\phi' & \cos\theta' \end{pmatrix}\mathbf{X} \qquad \text{(A2)}$$

$$\hat{n}_{X'} = \mathbf{A}\cdot\hat{n}_X = \begin{pmatrix} \cos\theta'\cos\phi' & \cos\theta'\sin\phi' & -\sin\theta' \\ -\sin\phi' & \cos\phi' & 0 \\ \sin\theta'\cos\phi' & \sin\theta'\sin\phi' & \cos\theta' \end{pmatrix}\cdot\begin{pmatrix} \sin\theta\cos\phi \\ \sin\theta\sin\phi \\ \cos\theta \end{pmatrix} \qquad \text{(A3)}$$

$$g_{\text{eff}}^{b-\text{heme}} = [\hat{n}_{X'}^{T}(g\cdot g^{T})\hat{n}_{X'}]^{1/2} = (g_z^{f2}\cos^2\eta + g_x^{f2}\sin^2\eta\cos^2\epsilon + g_y^{f2}\sin^2\eta\sin^2\epsilon)^{1/2} \qquad \text{(A4)}$$

Appendix II

To introduce the exchange coupling into the dipolar model, we begin with Bloembergen and co-worker's treatment of cross relaxation.[8] Consider the general spin Hamiltonian

$$\hat{H} = \hat{H}_z + \hat{H}_{cf} + \hat{H}_{sp-sp} \qquad \text{(A5)}$$

where the three terms on the right-hand side are the Zeeman term $\hat{H}_z$, the crystal field plus quadrupolar term $\hat{H}_{cf}$, and the generalized spin−spin interaction $\hat{H}_{sp-sp}$, respectively. For the

generalized spin−spin interaction between the two spins, $\hat{H}_{12}$ contains dipolar ($g_1g_2\ \beta^2/r_{12}^3$) and pseudodipolar (B_{12}) terms, and it has the explicit form

$$\hat{H}_{\mathrm{sp-sp}} = \boldsymbol{A} + \boldsymbol{B} + \boldsymbol{C} + \boldsymbol{D} + \boldsymbol{E} + \boldsymbol{F} \tag{A6}$$

with

$$\boldsymbol{A} = \left[\left(\frac{g_1g_2\beta^2}{r_{12}^3} + B_{12}\right)(1 - 3\cos^2\theta_{12})\right]S_{1Z}S_{2Z}$$

$$\boldsymbol{B} = \frac{1}{4}\left[\left(\frac{g_1g_2\beta^2}{r_{12}^3} + B_{12}\right)(1 - 3\cos^2\theta_{12})\right](S_{1+}S_{2-} + S_{1-}S_{2+})$$

$$\boldsymbol{C} = \frac{-3}{2}\left(\frac{g_1g_2\beta^2}{r_{12}^3} + B_{12}\right)\sin\theta_{12}\cos\theta_{12}\exp(-i\phi_{12})(S_{1+}S_{2Z} + S_{1Z}S_{2+})$$

$$\boldsymbol{D} = \frac{-3}{2}\left(\frac{g_1g_2\beta^2}{r_{12}^3} + B_{12}\right)\sin\theta_{12}\cos\theta_{12}\exp(i\phi_{12})(S_{1-}S_{2Z} + S_{1Z}S_{2-})$$

$$\boldsymbol{E} = \frac{-3}{4}\left(\frac{g_1g_2\beta^2}{r_{12}^3} + B_{12}\right)\sin^2\theta_{12}\exp(-2i\phi_{12})S_{1+}S_{2+}$$

$$\boldsymbol{F} = \frac{-3}{4}\left(\frac{g_1g_2\beta^2}{r_{12}^3} + B_{12}\right)\sin^2\theta_{12}\exp(2i\phi_{12})S_{1-}S_{2-}$$

With $B_{12} = 0$, the spin−spin interaction reduces to dipolar interaction. When the interspin distance becomes sufficiently short, we need to add the exchange contribution $\hat{H}_{\mathrm{ex}}$ to the Hamiltonian:

$$\hat{H}_{\mathrm{ex}} = \mathbf{S}_1\cdot\mathbf{J}\cdot\mathbf{S}_2 = (S_{1x}\ \ S_{1y}\ \ S_{1z})\begin{pmatrix} J_{xx} & J_{xy} & J_{xz} \\ J_{yx} & J_{yy} & J_{yz} \\ J_{zx} & J_{zy} & J_{zz} \end{pmatrix}\begin{pmatrix} S_{2x} \\ S_{2y} \\ S_{2z} \end{pmatrix} \tag{A7}$$

where *x, y, z* denote a set of axes fixed onto the molecular frame. To convert $\hat{H}_{\mathrm{ex}}$ to the laboratory frame, the J-tensor can be transformed to $\mathbf{J}' = \mathbf{n}^{\mathbf{T}}\cdot\mathbf{J}\cdot\mathbf{n}$, where **n** is similar to the rotation matrix **A** introduced in Appendix I (eq A2). Thus, eq A7 can be rewritten as

$$\hat{H}_{\mathrm{ex}} = \mathbf{S}_1\cdot\mathbf{J}'\cdot\mathbf{S}_2 = (S_{1X}\ \ S_{1Y}\ \ S_{1Z})\mathbf{J}'\begin{pmatrix} S_{2X} \\ S_{2Y} \\ S_{2Z} \end{pmatrix}$$

$$= (S_{1X}\ \ S_{1Y}\ \ S_{1Z})\begin{pmatrix} J'_{XX} & J'_{XY} & J'_{XZ} \\ J'_{YX} & J'_{YY} & J'_{YZ} \\ J'_{ZX} & J'_{ZY} & J'_{ZZ} \end{pmatrix}\begin{pmatrix} S_{2X} \\ S_{2Y} \\ S_{2Z} \end{pmatrix} \tag{A8}$$

As usual, $\mathbf{J}'$ can be separated into a scalar part, a polar vector, and a symmetric traceless tensor. When eq A8 is expanded, different terms in J′-tensor contribute to the various terms of the dipolar Hamiltonian ($\boldsymbol{A} - \boldsymbol{F}$ terms in eq A6). Specifically, only J'_{XX} and J'_{YY} of exchange coupling contribute to the *B* term (J^{B}). Note that all terms in the J′-tensor are angle-dependent and vary with the orientation of the *b*-heme with respect to the interspin vector.

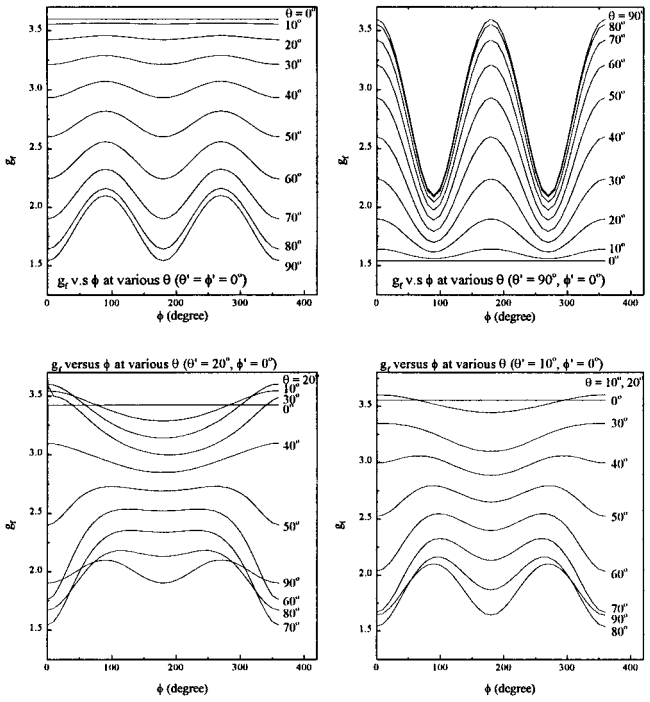

Figure 12. The dependence of g_{f} (*b*-heme) on θ and ϕ at several (θ', ϕ') orientations.

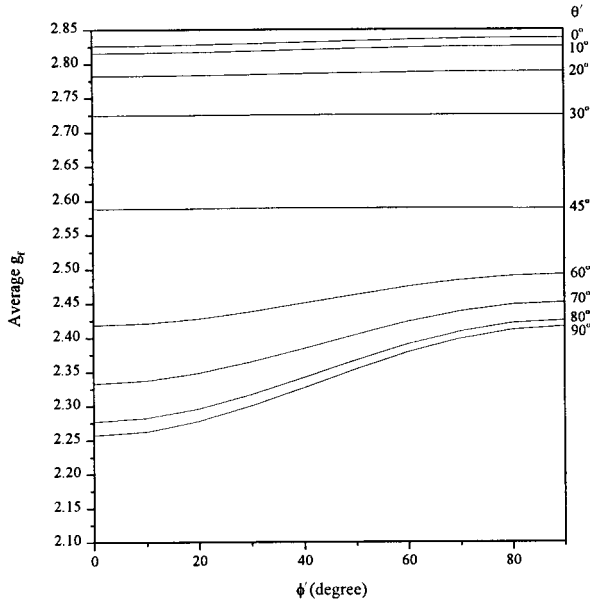

Figure 13. Averaged g_{f} (*b*-heme) as a function of the *b*-heme orientation with respect to the interspin vector (θ', ϕ').

Appendix III

The contributions of **b**, **c**, **e** terms in eq 13 were integrated over θ and ϕ at a specific orientation (θ', ϕ') of the *b*-heme with respect to the interspin vector (Figure 7). In turn, g_{f} can be expressed as a function of these four angles, θ, ϕ, θ', and ϕ' (Appendix I), where the g_x, g_y, and g_z of the *b*-heme are 1.5, 2.1, and 3.6, respectively.

Here, g_{f} is a function of θ and ϕ at a specific orientation of θ', ϕ'; therefore, the three terms, **b**, **c**, and **e**, which are functions of g_{f}, are also dependent on these four angles. In Figure 12, g_{f} is plotted versus ϕ at various θs. The g_{f} ranges from 1.5 (g_x) to 3.6 (g_z) for different (θ', ϕ') orientations. (The averaged g_{f} is also plotted versus ϕ' at various θ's in Figure 13.) Similarly, for each combination of θ' and ϕ', **b**, **c**, and **e** terms can be

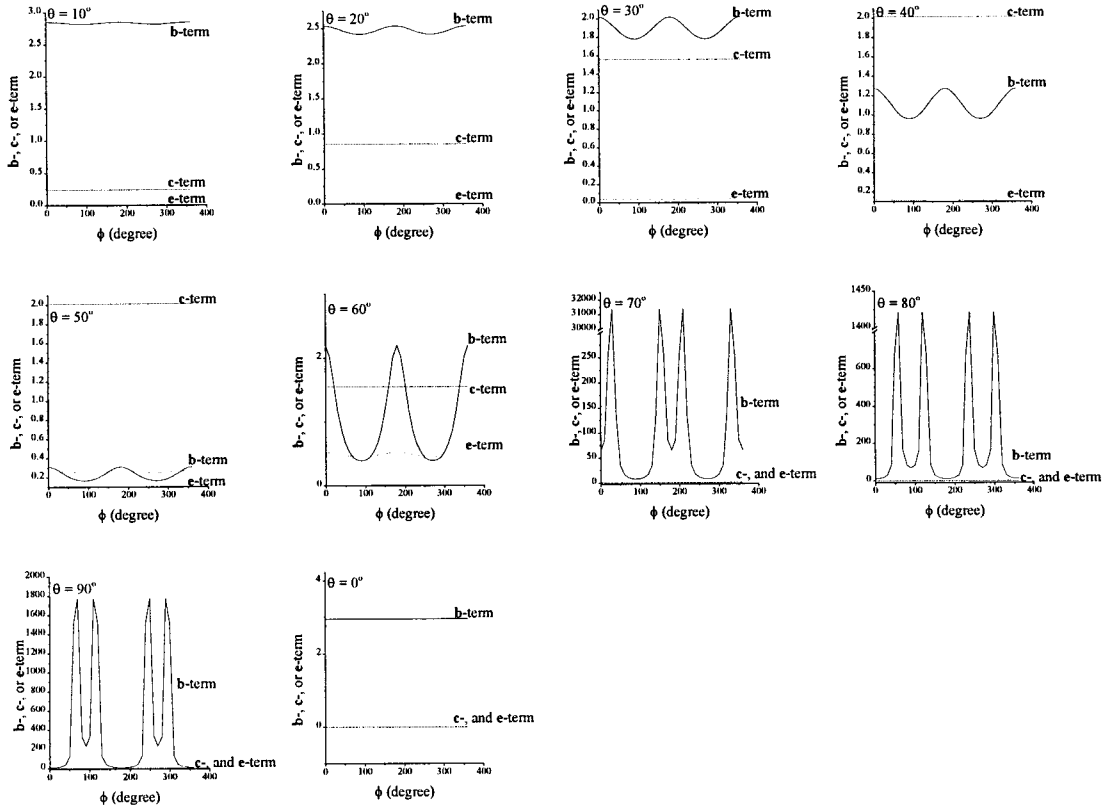

Figure 14. Comparison of the magnitude of **b**, **c**, and **e** terms of eq 14; **b** (solid line), **c** (dashed line), and **e** term (dotted line). Values are plotted versus ϕ at various θs. $T_{1f} = T_{2f} = 10^{-7}$s, and $\theta' = \phi' = 0°$.

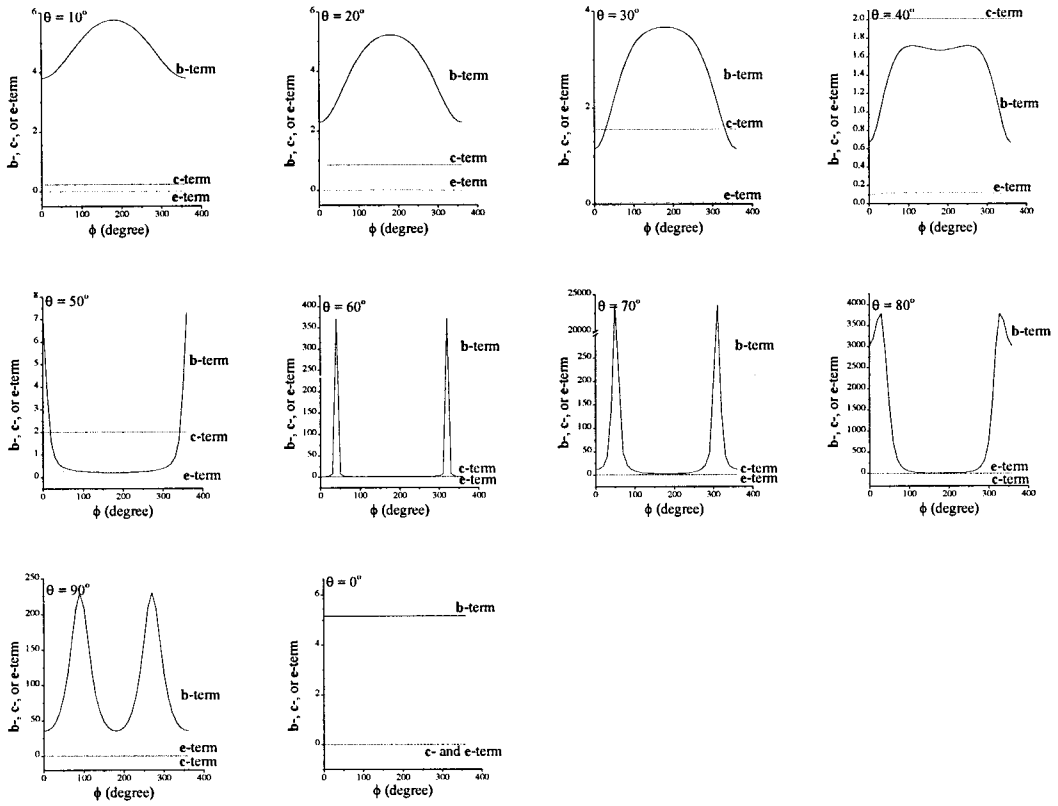

Figure 15. Comparison of the magnitude of **b**, **c**, and **e** terms of eq 14; **b** (solid line), **c** (dashed line), and **e** term (dotted line). Values are plotted versus ϕ at various θs. $T_{1f} = T_{2f} = 10^{-7}$ s, and $\theta' = 30°$, $\phi' = 0°$.

plotted as a function of ϕ for various θs (Figure 14 for $\theta' = \phi' = 0°$; Figure 15, for $\theta' = 30°$, $\phi' = 0°$; and Figure 16, for $\theta' = 90°$, $\phi' = 0°$) and assuming $T_{1f} = T_{2f} = 0.1\ \mu$s. The dominance of the **b** term will not be valid when $(1-3\cos^2\theta)/6 < 3\sin^2\theta\cos^2\theta$, which normally occurs at $\theta = 40°\sim60°$ and $120°\sim140°$. However, for the majority of the θ and ϕ region, the **b** term dominates. Therefore, for each integration over θ and ϕ in eq 13, **b** term dominates.

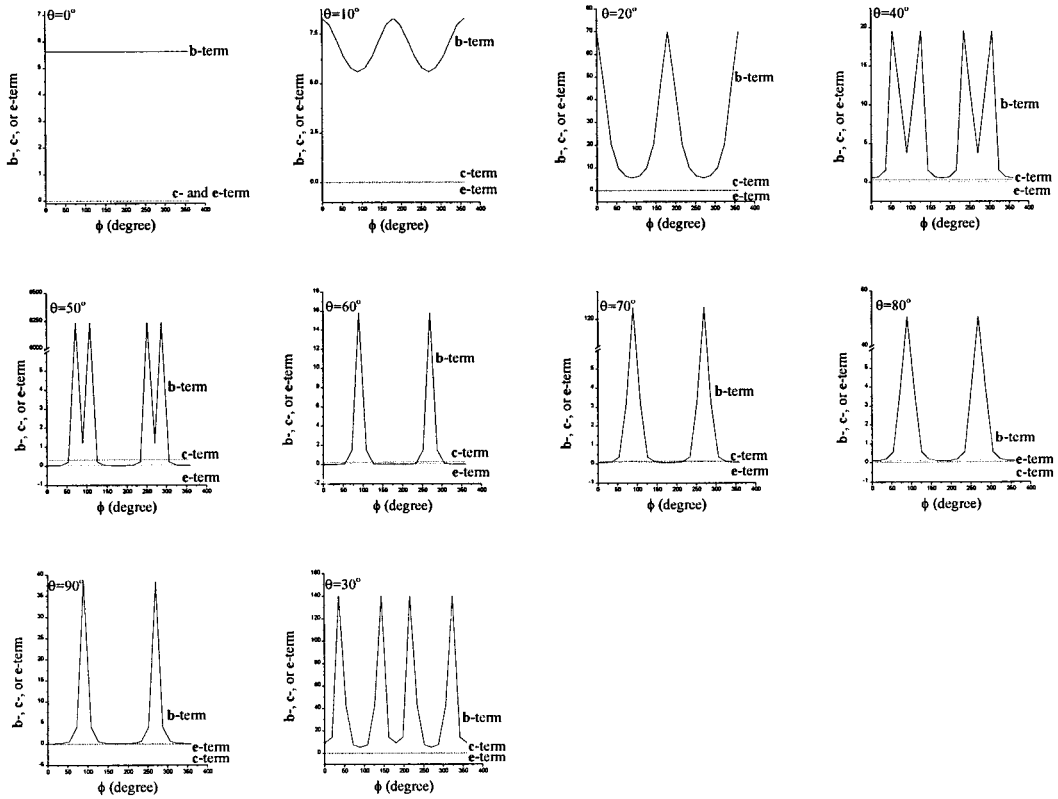

Figure 16. Comparison of the magnitude of **b**, **c**, and **e** terms of eq 14; **b** (solid line), **c** (dashed line), and **e** term (dotted line). Values are plotted versus ϕ at various θs. $T_{1f} = T_{2f} = 10^{-7}$ s, and $\theta' = 90°$, $\phi' = 0°$.

References and Notes

(1) Ackrell, B. A. C.; Johnson, M. K.; Gunsalus, R. P.; Cecchini, G. Structure and function of succinate dehydrogenase and fumarate reductase. In *Chemistry and biochemistry of flavoenzymes*; Müller, F., Ed.; CRC Press: Boca Raton, 1992; Vol. III, pp 229−297.

(2) Allen, J. P.; Colvin, J. T.; Stinson, D. G.; Flynn, C. P.; Stapleton, H. J. *Biophys. J.* **1982**, *38*, 299.

(3) Banci, L.; Bertini, I.; Luchinat, C. *Nuclear and electron relaxation*; VCH: New York, 1991.

(4) Beck, W. F.; Innes, J. B.; Lynch, J. B.; Brudvig, G. W. *J. Magn. Reson.* **1991**, *91*, 12.

(5) Berry, E. A.; Trumpower, B. L. *J. Biol. Chem.* **1985**, *260*, 2458.

(6) Berry, E. A.; Trumpower, B. L. *Anal. Biochem.* **1987**, *161*, 1.

(7) Bertrand, P.; Guigliarelli, B.; Meyer, J.; Gayda, J.-P. *Biochimie* **1984**, *66*, 77.

(8) Bloembergen, N.; Shapiro, S.; Pershan, P. S.; Artman, J. O. *Phys. Rev.* **1959**, *114*, 445.

(9) Brudvig, G. W.; Blair, D. F.; Chan, S. I. *J. Biol. Chem.* **1984**, *259*, 11001.

(10) Cheng, C.; Lin, T.-S.; Sloop, David J. *J. Magn. Reson.* **1979**, *33*, 71.

(11) Dalton, L. R., Thesis, Harvard University, 1971.

(12) Galli, C.; Innes, J. B.; Hirsh, D. J.; Brudvig, G. W. *J. Magn. Reson.* **1996**, *B110*, 284.

(13) Gayda, J.-P.; Bertrand, P.; Theodule, F.-X. *J. Chem. Phys.* **1982**, *77*, 3387.

(14) Goodman, G.; Leigh, J. S. J. *Biochemistry* **1985**, *24*, 2310.

(15) Guigliarelli, B.; More, C.; Bertrand, P.; Gayda, J.-P. *J. Chem. Phys.* **1986**, *85*, 2774.

(16) Hägerhäll, C. *Biochim. Biophys. Acta* **1997**, *1320*, 107.

(17) Hederstedt, L.; Ohnishi, T. Progress in succinate:quinone oxidoreductase research. In *Molecular mechanisms in bioenergetics*; Ernster, L., Ed.; Elsevier Science Publishers: Amsterdam, 1992; pp 163−198.

(18) Hirsh, D. J.; Brudvig, G. W. *J. Phys. Chem.* **1993**, *97*, 13216.

(19) Houseman, A. L. P.; Doan, P. E.; Goodin, D. B.; Hoffman, B. M. *Biochemistry* **1993**, *32*, 4430.

(20) Iverson, T. M.; Luna-Chavez, C.; Cecchini, G.; Rees, D. C. *Science* **1999**, *284*, 1961.

(21) Koptyug, I. V.; Bossmann, Stefan H.; Turro, Nicholas J. *J. Am. Chem. Soc.* **1996**, *118*, 1435.

(22) Kulikov, A. V.; Likhtenstein, G. I. *Adv. Mol. Relax. Interact. Processes* **1977**, *10*, 47.

(23) Lorigan, G. A.; Britt, R. D. *Biochemistry* **1994**, *33*, 12072.

(24) Matsson, M.; Ackrell, B. A. C.; Cochran, B.; Hederstedt, L. *Arch. Microbiol.* **1998**, *170*, 27.

(25) Ohnishi, T. *Curr. Top. Bioenerg.* **1987**, *15*, 37.

(26) Pennoyer, J. D.; Ohnishi, T.; Trumpower, B. L. *Biochim. Biophys. Acta* **1988**, *935*, 195.

(27) Rakowsky, M. H.; More, K. M.; Kulikov, A. V.; Eaton, G. R.; Eaton, S. S. *J. Am. Chem. Soc.* **1995**, *117*, 2049.

(28) Shergill, J. K.; Cammack, R.; Weiner, J. H. *J. Chem. Soc., Faraday Trans.* **1991**, *87*, 3199.

(29) Steffens, G. C. M.; Pascual, E.; Buse, G. *J. Chromatogr.* **1990**, *521*, 291.

(30) Stowell, M. H. B.; Larsen, R. W.; Winkler, J. R.; Rees, D. C.; Chan, S. I. *J. Phys. Chem.* **1993**, *97*, 3054.

(31) Sturgeon, B. E.; Britt, R. D. *Rev. Sci. Instrum.* **1992**, *63*, 2187.

(32) Waldeck, A. R.; Stowell, M. H. B.; Lee, H. K.; Hung, S.-C.; Matsson, M.; Hederstedt, L.; Ackrell, B. A. C.; Chan, S. I. *J. Biol. Chem.* **1997**, *272*, 19373.

(33) Wilson, D. F.; King, T. E. *J. Biol. Chem.* **1964**, *239*, 2683.